

The Angular Dependence of $^{16}\text{O}(e, e'K^+)_{\Lambda}^{16}\text{N}$ and $\text{H}(e, e'K^+)_{\Lambda}$

(Proposal to JLab PAC-31)

**E. Cisbani, F. Cusanno, S. Frullani,
F. Garibaldi (spokesperson and contact person), M.L. Magliozzi**

*Istituto Nazionale di Fisica Nucleare, Sezione di Roma, Gr. Coll. Sanita',
Viale Regina Elena 299, Rome, Italy*

M. Iodice (co-spokesperson)

Istituto Nazionale di Fisica Nucleare, Sezione di Roma Tre, I-00146 Roma, Italy

G.M. Urciuoli

Istituto Nazionale di Fisica Nucleare, Sezione di Roma1, Piazza A. Moro, Rome, Italy

A. Acha, P. Markowitz (co-spokesperson)

Florida International University, Miami, Florida 33199, USA

C.C. Chang

University of Maryland, College Park, Maryland 20742, USA

J.P.Chen, D.Higinbotham J.J. LeRose (co-spokesperson), A.Saha, B.Wojtsekhowski

Thomas Jefferson National Accelerator Facility, Newport News, Virginia 23606, USA

P. Bydžovský, M. Sotona

Nuclear Physics Institute, Řež near Prague, Czech Republic

R. De Leo, L. Lagamba, S. Marrone

Istituto Nazionale di Fisica Nucleare, Sezione di Bari and University of Bari, I-70126 Bari, Italy

D.J. Millener

Brookhaven National Laboratory, Upton, New York 11973, USA

H.J.Schulze

Istituto Nazionale di Fisica Nucleare, Sezione di Catania, I-95123 Catania, Italy

December 9, 2006

Submitted to The JLab PAC-31

by the

Hall A Kaon Collaboration - Approval as a Hall A Collaboration is pending

Abstract

In all Jlab hypernuclear electroproduction experiments already performed (E89-009, E94-107, E01-011) or approved (E05-015) the K^+ mesons are detected at very small (few degrees) laboratory scattering angles (measured with respect to virtual photon momentum). This region of kaon scattering angles is not covered, unfortunately, by recent photo- and electroproduction data on the elementary production process from CLAS, SAPHIR, and LEPS Collaborations. The angular dependences of the cross section at small angles and at photon energies $E_\gamma \approx 2$ GeV predicted by different models for the $K^+\Lambda$ electromagnetic production differ drastically and this lack of relevant information about the elementary process makes an interpretation of obtained hypernuclear spectra difficult. In addition, the ratio of the hypernuclear (calculated in DWIA) and elementary cross section measured at the same kinematics should be almost model independent at very forward kaon scattering angles. The ratio therefore contains direct information on the target and hypernuclear structure, production mechanisms and, possibly, on the modification of the dynamics of the elementary $p(e, e'K^+)\Lambda$ process in the nuclear environment.

The Hall A experimental setup with septum magnets has a unique opportunity to solve the above mentioned problems using the waterfall target and virtual photons with energy $E_{\gamma^*} \simeq 2$ GeV. We will measure:

- the electroproduction cross section on the proton in H_2O at LAB kaon scattering angles $\theta_{Ke}^{LAB} = 8.5^\circ$ and 11° ($\theta_{K\gamma}^{LAB} = 4^\circ$ and 7°) which together with our previous measurements for $\theta_{Ke}^{LAB} = 6^\circ$ ($\theta_{K\gamma}^{LAB} = 2^\circ$) will cover the angular region missing in CLAS and SAPHIR data. New precise data will clearly discriminate between various models of photo- and electroproduction of strangeness, such as Saclay-Lyon and Kaon-MAID;
- the angular dependence of the hypernuclear cross section (HN) on ^{16}O will be determined simultaneously. These data and, especially, the ratio of HN to the elementary cross section will give new valuable information on hypernuclear structure (including spin assignment of produced hypernuclear states), reaction mechanisms and, may be, the modification of the dynamics of the $(e, e'K^+)\Lambda$ process in the nuclear medium.

1 High Resolution Hypernuclear Spectroscopy

The physics of hypernuclei - multibaryonic systems with non-zero strangeness - is an important branch of contemporary nuclear physics at low energy (structure, energy spectra and weak decays of hypernuclei) as well as at intermediate energy (production mechanism). The Λ hypernucleus is a long living baryon system ($\tau \approx 10^{-10} \text{ sec}$) and provide us with a variety of nuclear phenomena. The strange quark is an impurity in the system that allows measuring the system response to the stress imposed by it. The study of its propagation can reveal configurations or states not seen in other ways. The study also gives important insight into the structure of ordinary nuclear matter. The hyperon is not affected by Pauli principle and can penetrate deep inside the nucleus. More generally the nucleus provides a unique laboratory for studying the Λ - N interaction. In addition, there is growing evidence of the hyperon's importance in cosmology. The appearance of hyperons usually lowers dramatically the maximum possible mass of a stable neutron star, even below the maximum observed values of about 1.5 solar masses. This would be a strong indication for the presence of non-hadronic, i.e., "quark" matter inside the star. It could thus be the first indirect "proof" of the existence of quark matter in nature. In order to draw firm conclusions regarding this aspect, it is necessary to perform precise microscopic calculations of the equation of state of dense hadronic matter, including hyperons. Brueckner calculations of hypernuclear matter have achieved a high degree of sophistication and precision and require as input equally precise baryon-baryon potentials.

From low-energy Λp scattering studies we obtained information about the s -state ΛN interaction but the noncentral part of ΛN forces is not well established. Especially useful information comes from the spin dependent part of the interaction.

An effective ΛN interaction can be determined from hypernuclear (HN) energy spectra obtained from various reactions. This information can then be used to discriminate between various bare hyperon - nucleon and hyperon - hyperon potentials treated in Brueckner reaction matrix approach.

Summarizing, the detailed knowledge of the ΛN interaction is important for the following reasons:

- It provides a check of various generalized models of the baryon - baryon interaction (including hyperons) based on effective field theory (Nijmegen, Jülich, ... potentials) and on quark motivated attempts to describe the short range part of this interaction.
- By comparing the energy spectra of "mirror" hypernuclei, such as ${}^{12}_{\Lambda}\text{C} - {}^{12}_{\Lambda}\text{B}$, ${}^{16}_{\Lambda}\text{O} - {}^{16}_{\Lambda}\text{N}$, one can, in principle, extract some additional information about charge symmetry breaking part of ΛN interaction which has been seen many years ago in ${}^4_{\Lambda}\text{H} - {}^4_{\Lambda}\text{He}$ case??.

- More precise knowledge of the hyperon - nucleon and hyperon - hyperon interaction can shed some light on the role of strange quarks in the dynamics of the low- and intermediate energy baryonic systems.
- Hyperons appear to be the first of strange hadrons in neutron stars, occurring at around the normal nuclear density. It is necessary to perform precise microscopic calculations of the equation of state of dense hadronic matter, including hyperons. Brueckner calculations of hypernuclear matter require as input precise baryon-baryon potentials. Hyperon-nucleon potentials are still not very well constrained by data, and a more accurate measurement of hypernuclear levels (in particular in neutron-rich nuclei) will allow to narrow the margin of uncertainty associated with these forces so far.

1.1 Hypernuclear Spectroscopy with hadronic probes

Λ -hypernuclei can be produced and studied with a wide variety of hadron probes, such as mesons (K^- , π), protons, and heavy ions. Especially meson beams have been widely used in hypernuclear investigations. The K^- beam with momentum $p_K = 700 - 900$ MeV/c and hypernuclear production cross section ~ 10 mb/sr was used in pioneering experiments at CERN. The production cross section with a π^+ beam at momentum $P_\pi = 1.04$ GeV/c (the elementary cross section of $\pi^+ + n \rightarrow \Lambda + K^+$ has a maximum at this momentum) is much smaller ~ 10 μ b/sr but much higher intensities of pion beams can compensate this smaller cross section. The first BNL experiments with a π^+ beam [3] were followed by precise experiments at KEK with much better energy resolution $\sim 1.5 - 2$ MeV - see the review [1] and references therein.

The situation for experiments with meson beams is as follows:

- The non-spin-flip (K^-, π^-) reaction strongly populates substitutional states at low momentum transfers near 0° ($q \sim 100$ MeV/c). Higher angular momentum states are populated at larger angles. The reaction is now used mainly in connection with γ -ray spectroscopy
- The momentum transfer for (π^+, K^+) reaction is very similar to that for the ($e, e'K^+$) reaction but the spin-flip amplitudes are weak and only low-spin members of doublets are populated significantly on a J=0 target.
- For (K_{stop}^-, π^-) capture at rest with $q \sim 200$ MeV/c, the situation is similar to that for (π^+, K^+)

In the p -shell region high-statistics excitation spectra were determined from the (π^+, K^+) reaction at KEK for ${}^7_\Lambda\text{Li}$, ${}^9_\Lambda\text{Be}$, ${}^{12}_\Lambda\text{C}$, ${}^{13}_\Lambda\text{C}$, and ${}^{16}_\Lambda\text{O}$ hypernuclei including the angular dependence of the cross sections. The data were compared with DWIA calculations using shell model transition densities with a phenomenological $\Lambda - N$ interaction.

The (π^+, K^+) reaction was then used to map out the mass dependence of hypernuclei beyond the p -shell region - from ${}^{28}_{\Lambda}\text{Si}$ up to hypernuclei as heavy as ${}^{208}_{\Lambda}\text{Pb}$, where the g_{Λ} orbit is bound. The mass dependence confirmed that, at least in first approximation, Λ hyperon keeps its identity even in the deeply bound single particle states.

1.1.1 Gamma Spectroscopy.

The situation was improved by introducing the standard tool of conventional nuclear physics - γ spectroscopy. That is coincidence experiments, e.g. $(K^-, \pi^-\gamma)$ and $(\pi^+, K^+\gamma)$, with a few keV energy resolution, see Ref. [1] and references therein. High precision data were obtained for a number of electromagnetic transitions in ${}^7_{\Lambda}\text{Li}$, ${}^9_{\Lambda}\text{Be}$, ${}^{10}_{\Lambda}\text{B}$, ${}^{11}_{\Lambda}\text{B}$, ${}^{13}_{\Lambda}\text{C}$, ${}^{15}_{\Lambda}\text{N}$, and ${}^{16}_{\Lambda}\text{O}$ hypernuclei. In particular, the parameters of spin-spin, Λ -spin-orbit, nucleon-spin-orbit and tensor $\Lambda - N$ p -shell residual interaction were determined from ${}^7_{\Lambda}\text{Li}(3/2^+, 1/2^+)$, ${}^7_{\Lambda}\text{Li}(7/2^+, 5/2^+, 3/2^+, 1/2^+)$, ${}^9_{\Lambda}\text{Be}(3/2^+, 5/2^+)$, and ${}^{16}_{\Lambda}\text{O}(1^-, 0^-)$ spacings. Other data from (π^+, K^+) spectroscopy (e.g. ${}^{12}_{\Lambda}\text{C}$ energy spectra) are also consistent with this set of $\Lambda - N$ interaction parameters and it seemed that at least for p -shell hypernuclei everything is done and known. However, recent γ -ray spectroscopy of level spacings in ${}^{10}_{\Lambda}\text{B}$ and ${}^{11}_{\Lambda}\text{B}$ hypernuclei seems to destroy this nice picture and further experimental and theoretical effort is needed to understand hypernuclear structure, in particular the role of $\Lambda N \rightarrow \Sigma N$ strong mixture in hypernuclei.

In addition, only the states strongly populated in (K^-, π^-) or (π^+, K^+) may be studied by γ -ray spectroscopy and, as we already mentioned, the number of such states is limited by weak spin flip.

1.2 Hypernuclear Spectroscopy with Electromagnetic Probes

Experimental knowledge can be extended by electroproduction of strangeness characterized by large momentum transfer ($q \geq 250$ MeV/c; see Fig. 5 of Ref. [1]) and strong spin-flip terms even at zero kaon production angle. Photons (real or virtual) may excite both natural and unnatural parity, as well as low-spin and high-spin hypernuclear states including states with a deeply-bound Λ hyperon. In the electromagnetic case, the spin-flip transitions are strong, meaning that both members of doublets are populated. In addition, the reaction takes place on the proton while with hadron probes (K^- and π^+) it takes place on the neutron, so new hypernuclei are created. The disadvantage of smaller electromagnetic cross sections is partially compensated by the high current, continuous, and high energy resolution of the beam at Jefferson Laboratory

Summarizing the main merits of the electro-magnetic production:

- high intensity and excellent energy resolution of electron beam make possible to identify hypernuclear levels with a resolution of the order of few hundred keV;

- photo- and electro-production reactions are characterized by the large momentum transfer ($q \geq 250$ MeV/c) and the strong spin-flip terms even at zero kaon production angles. This means that photons (real or virtual) can therefore excite both natural and unnatural parity, low- and high-spin hypernuclear states including states with deeply-bound Λ hyperons;
- in contrast to (K^-, π^-) or (π^+, K^+) , electromagnetic production of $K^+\Lambda$ pair goes on the proton which allows studying hypernuclei not available otherwise (${}^{12}_{\Lambda}\text{B}$) including hypernuclei with large excess of neutral baryons (${}^7_{\Lambda}\text{He}$, ${}^9_{\Lambda}\text{Li}$). Comparison of the spectra of *mirror* hypernuclei, e.g. ${}^{12}_{\Lambda}\text{B} - {}^{12}_{\Lambda}\text{C}$, can then shed some light on the charge asymmetry of hyperon - nucleon forces;
- the production of controversial Σ -hypernuclei is another interesting problem for the electroproduction of strangeness since the Σ and Λ production rates are comparable in this process.

So new, precise hypernuclear spectroscopic data obtained at Jefferson Laboratory can contribute to improvement in our understanding of hadron - hadron dynamics.

2 Results from previous experiments on hypernuclear electro-production at JLab

The first CEBAF electroproduction experiment, E89-009, proved that the electroproduction process can be effectively used to study HN spectra with energy resolutions less than 1 MeV. However, due to the rather low statistics only the ground state doublet peak and another peak at excitation energy $E_x \sim 11\text{MeV}$ corresponding to Λ hyperon in $1p$ state can be resolved. Moreover, statistics were not sufficient to recognize predicted core excited states.

The Hall C collaboration significantly improved the apparatus and performed another experiment (E01-011) (${}^{12}\text{C}$, ${}^9\text{Be}$, ${}^{28}\text{Si}$..) and was approved for a third (E05-115).

At the same time, our group (Hall A kaon collaboration) performed experiment E94-107 [2] on ${}^{12}\text{C}$, ${}^{16}\text{O}$ and ${}^9\text{Be}$.

In Fig. 1 the excitation energy spectrum of ${}^{12}_{\Lambda}\text{B}$ is shown for the full range of energy acceptance. The filled histogram shows the level of (e, e') , (e, K^+) random coincidence background. The ${}^{12}\text{C}$ results show that a high quality, background free ${}^{12}_{\Lambda}\text{B}$ hypernuclear spectrum with unprecedented energy resolution (~ 640 keV) has been obtained.

Figure 2 shows the six-fold differential cross section expressed in $\text{nb}/(\text{sr}^2/\text{GeV MeV})$. The background has been evaluated by fitting the data obtained for random coincidences in a large timing window and subtracted. No residual background in the negative range of E_x is present after subtraction.

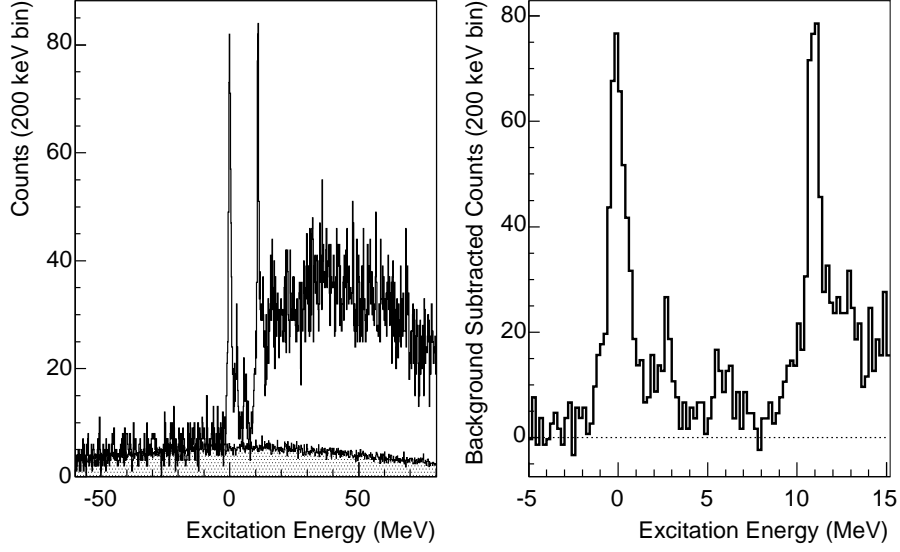


Figure 1: Left panel: $^{12}_{\Lambda}\text{B}$ excitation-energy spectrum as obtained after kaon selection with aerogel detectors and RICH without background subtraction. The electron kaon random coincidence contribution evaluated in a large timing window and normalized is superimposed on the spectrum. The unique feature of an almost background-free experiment can be observed. Right panel: exploded view of the hypernuclear bound state region with background subtracted.

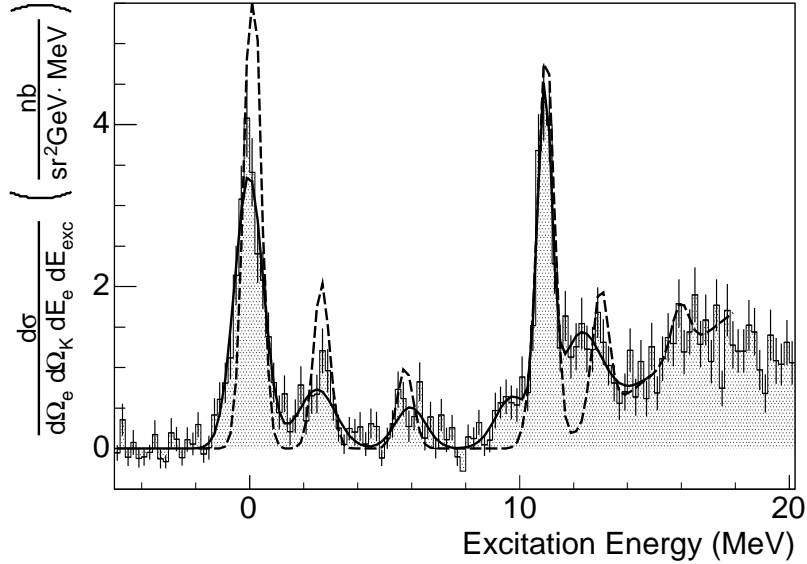


Figure 2: $^{12}_{\Lambda}\text{B}$ excitation-energy spectrum. The best fit and a theoretical curve are superimposed on the data. See text for details.

The solid line represents the best fit to the data. The dashed line is the result of a theoretical

model which shows very good overall agreement with the data without any normalization factor. Publications of these results is imminent.

One essential ingredient of any hypernuclear cross section calculation is the model for the elementary cross section of $K^+-\Lambda$ electroproduction on proton. Since counting rates for hypernuclear electroproduction decrease dramatically with increasing Q^2 and $\theta_{\gamma-K}$ these experiments at electron beam facilities are always carried out at very low Q^2 and with kaon detection at forward angles. As will be discussed in the following, this is exactly the region where there is a lack of precision data for the $p(e, e'K^+)\Lambda$ reaction and where the existing data show large discrepancies and also where models show very different behavior with huge differences in cross section predictions. This is one of the reasons why it is extremely important to carry out precise measurements of the $p(e, e'K^+)\Lambda$ reaction in this kinematical region.

The model that has been used to compare our data with the theory (dashed line in the figure) is obtained in the framework of the Distorted Wave Impulse Approximation (DWIA) [7] using the Saclay-Lyon (SLA) model [8] for the elementary $p(e, e'K^+)\Lambda$ reaction. Shell-model wave functions for ^{11}B and $^{12}_{\Lambda}\text{B}$ were obtained using fitted p -shell interactions and a parametrization of the ΛN interaction that fits the precise γ -ray spectra of $^7_{\Lambda}\text{Li}$ [26].

The very good agreement of the data with the predicted cross section is a first, though indirect, indication that the SLA model give a good description of the elementary cross section at Q^2 as low as $0.07 \text{ GeV}/c^2$ and at forward angle kaon detection.

For the first time a measurable strength with good energy resolution has been observed in the core-excited part of the spectrum. The s_{Λ} part of the spectrum is well reproduced by the theory. The distribution of strength within several MeV on either side of the strong p_{Λ} peak should stimulate theoretical work to better understand the p_{Λ} region.

A waterfall target has been used during experiment e94107 for hypernuclear production on oxygen nuclei as well as for the measurement of the elementary cross section $p(e, e'K^+)\Lambda$ on hydrogen nuclei.

Kinematics were set to electron detection at 6° for scattered electrons with momentum of $1.44 \text{ GeV}/c$, incident beam energy of 3.66 GeV , virtual photon energy of 2.2 GeV with $Q^2 = 0.06 \text{ GeV}^2$. Scattered kaons were detected with momenta of $1.96 \text{ GeV}/c$ at 6° . One of the main goal of the present proposal is to extend the measurement at larger angles $\theta_{K^+-\gamma}$ between the detected kaon and the virtual photon direction.

Figure 3 shows the preliminary data obtained for the $^{16}_{\Lambda}\text{N}$ hypernuclear spectrum produced on Oxygen nuclei at $Q_{K^+e} = 6^\circ$. The solid line is a result of the theoretical calculation obtained with the SLA model for the elementary cross section and by using J.Millener calculations for the hypernuclear structure. The theoretical curve has been normalized to the data at this stage of analysis. The overall picture shows a very good agreement between the data and the calculations,

especially in terms of positions and relative strength of the levels. However at the present stage of the analysis a discrepancy of a factor 2 between the data and the calculations is found in terms of absolute cross sections, the data suggesting smaller cross sections. This result is also consistent with previous (π^+, K^+) experiment carried out at KEK[1]

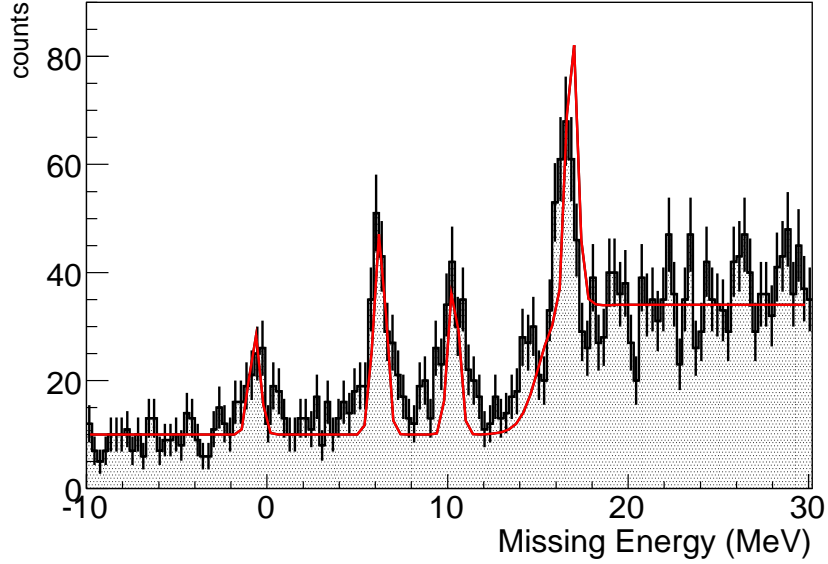


Figure 3: Preliminary data for the $^{16}_{\Lambda}\text{N}$ missing-energy spectrum.

In following table, the experimental cross sections from $(\pi^+.K^+)$ reaction (integrated over the angular range $\theta_K = 2^\circ - 14^\circ$) and from $(e, e'K^+)$ JLab experiment on ^{12}C and ^{16}O targets are compared with theoretical predictions (two sets of theoretical predictions differ in the assumed binding energy of p_Λ state - Wood-Saxon wave function is used for weakly bound p_Λ). One can see that in the case of ^{12}C target the agreement is surprisingly good but for ^{16}O target the theoretical predictions overestimate the data approximately by a factor 2 for low-energy hypernuclear states $\Lambda \in s_{1/2}$. Taking into account that the structure of closed shell ^{16}O target should be more simple then ^{12}C one this is rather surprising and at the moment we have no explanation for it.

The preliminary results on the simultaneous measurement of the elementary reaction on hydrogen shows also a similar discrepancy between the data ($\sigma=23\text{nb}/\text{sr}^2/\text{GeV} \pm 40\%$) with respect to the predicted cross section of $36 \text{ nb}/\text{sr}^2/\text{GeV}$ according to the SLA model.

This proposal is essential to also shed light on this observation.

HN levels		KEK (π^+, K^+)			E94-107 ($e, e'K^+$)	
$E_x(MeV)$	J^π	$\sigma_{2^\circ-14^\circ}^{exper}$	$\sigma_{2^\circ-14^\circ}^{theor1}$	$\sigma_{2^\circ-14^\circ}^{theor2}$	$d^3\sigma_{exper}$	$d^3\sigma_{theor}$
0.00	$1^-, 2^-$	1.44 ± 0.03	1.53	1.53	$4.47 \pm 0.21(st) \pm 0.58(sys)$	4.68
~ 2.65	1^-	0.24 ± 0.02	0.25	0.25	$1.26 \pm 0.11(st) \pm 0.16(sys)$	1.54
~ 6.00	$1^-, 2^-$	0.23 ± 0.02	0.16	0.16	$0.72 \pm 0.09(st) \pm 0.09(sys)$	0.76
8.12		0.18 ± 0.02				
9.77					$0.91 \pm 0.10(st) \pm 0.12(sys)$	
~ 11.0	$0^+, 2^+, 3^+$	1.81 ± 0.05	3.28	2.18	$2.90 \pm 0.17(st) \pm 0.38(sys)$	3.98
~ 12.2	2^+				$2.42 \pm 0.16(st)_{-0.73}^{+0.41}(sys)$	1.18

Table 1: (π^+, K^+) (KEK) and ($e, e'K^+$) (JLab E94-107) production on ^{12}C target compared with theoretical predictions

HN levels		KEK (π^+, K^+)			E94-107 ($e, e'K^+$)	
$E_x(MeV)$	J^π	$\sigma_{2^\circ-14^\circ}^{exper}$	$\sigma_{2^\circ-14^\circ}^{theor1}$	$\sigma_{2^\circ-14^\circ}^{theor2}$	$d^3\sigma_{exper}$	$d^3\sigma_{theor}$
0.000	1^-	0.41 ± 0.02	0.96	0.96	$1.3 \pm 40\%$	2.50
~ 6.5	$1^-, 2^-$	0.91 ± 0.03	1.68	1.68	$2.8 \pm 40\%$	4.54
~ 11	$1^+, 2^+$	1.05 ± 0.03	1.95	1.35	$2.5 \pm 40\%$	3.94
~ 17.5	$1^+, 2^+, 3^+$	1.38 ± 0.06	4.12	2.86	$3.8 \pm 40\%$	7.62

Table 2: (π^+, K^+) (KEK) and ($e, e'K^+$) (JLab E94-107 - PRELIMINARY results) production on ^{16}O targets compared with theoretical predictions

3 Proposed Measurements.

In all Jlab hypernuclear electroproduction experiments, which either were already performed (E89-009, E94-107, and E01-011) or are approved (E05-115), kaons are detected at very small laboratory angles $\theta_{K\gamma}$, measured with respect to virtual photon momentum, see Table 3 where θ_e and θ_{Ke} are angles measured versus the electron beam of the secondary electron and kaon, respectively.

Only in Hall A experiment E94-107 were Oxygen and Hydrogen measurements performed simultaneously using the waterfall target.

The cross section of ($e, e'K^+$) reactions on a complex nuclear target and its angular dependence are determined mainly by the following factors:

- by the transition operator, that is given by the model used to describe the elementary production on individual protons;

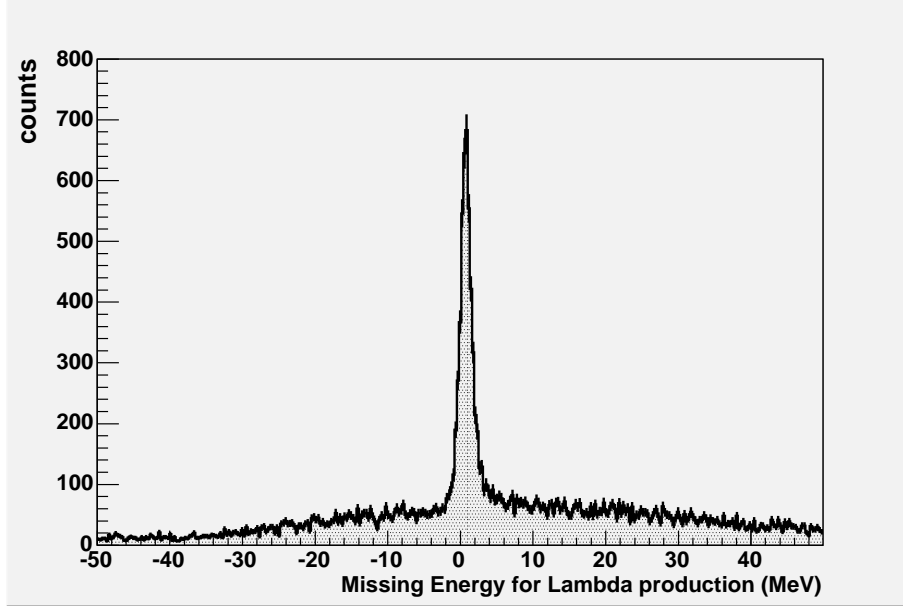


Figure 4: Preliminary data for the $p(e, e'K^+)\Lambda$ measured on the waterfall target in the experiment e94107.

Table 3: Comparison of kinematics of hypernuclear experiments in JLab.

	E89-009	E94-107	E01-011	E05-015
θ_e	≈ 0	6	≈ 0	≈ 0
θ_{Ke}	0 - 7	6	1 - 14.7	1 - 13
$\theta_{K\gamma}$	3	≈ 2	7	7

- by the structure (that is the many particle wave function) of the target nucleus and the produced hypernuclear state;
- by the momentum transferred to the nucleus $\vec{q} = \vec{p}_\gamma - \vec{p}_K$.

The angular dependence of the cross section is determined mainly by the momentum transferred to the nucleus (q) via the nucleus - hypernucleus transition form factor. q is a rapidly increasing function of the kaon scattering angle - see Fig. 5.

In principle the angular dependence is influenced also by an angular dependence in the elementary production operator but at virtual photon energies $E_\gamma \approx 2$ GeV it is as a rule weak - see however discussion in Sec. (3.1). One can show easily [7] that at very forward kaon scattering angles ($\sin^2 \theta_{K\gamma} \ll 1$) the elementary as well as the transverse part of the hypernuclear electroproduction cross section is proportional to the same combination $|f_1 - f_2|^2$ of CGLN amplitudes. However, at electron kinematics used in the electroproduction

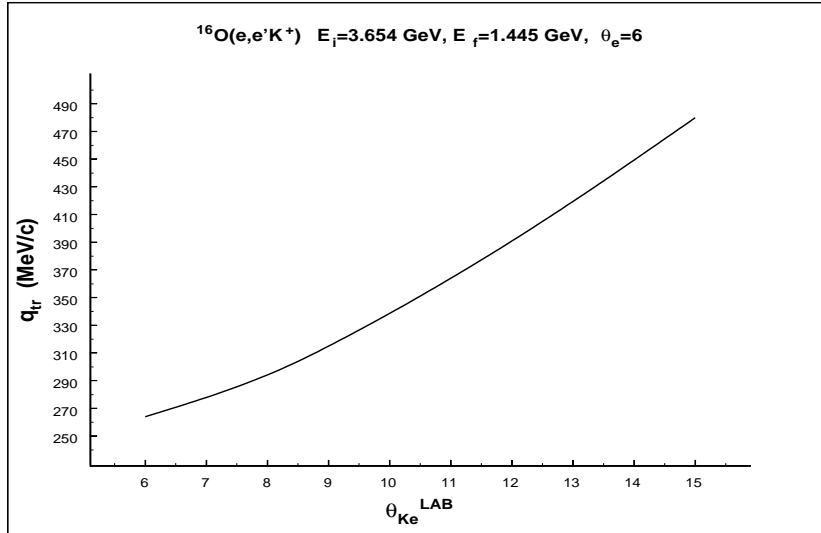


Figure 5: Momentum transferred to the nucleus in the $^{16}\text{O}(e, e'K^+)^{16}_{\Lambda}\text{N}$ reaction as a function of kaon scattering angle θ_{Ke} . Beam energy $E_i = 3.66$ GeV, secondary electrons energy $E_f = 1.44$ GeV, electron scattering angle $\theta_e = 6^\circ$.

of hypernuclei (small electron scattering angle) the other parts (longitudinal and interference terms) of the electroproduction cross section should be negligible. This means that the ratio of the hypernuclear and elementary cross section does not depend on the electroproduction model and contains therefore direct information on hypernuclear structure, production mechanism, and possibly on modification of the dynamics of the elementary process in the nuclear environment. Simultaneous determination of the hypernuclear and elementary electroproduction cross sections (e.g. on the waterfall target) can therefore shed new light on the problem.

Measurements using the waterfall target make it possible to simultaneously collect data for two different processes: the production of $^{16}_{\Lambda}\text{N}$ hypernucleus and the elementary process on the proton. We will take advantage of this possibility and measure an angular dependence of the cross section for the hypernucleus production and the cross section for electro-production of kaons on the proton for very small kaon angles. This is difficult to achieve in any other experimental setup.

3.1 Measurement of the Cross Section for Kaon Electro-Production on the Proton at Very Forward Angle and Very Small Q^2

The process of photo- and electro-production of kaons on the proton in the resonance region is usually described in the framework of the hadrodynamical effective field formalism, where the standard perturbation expansion is limited to the tree-level approximation, see e.g. Refs.

[8, 9, 10, 11]. The relevant degrees of freedom are nucleon, kaon and hyperon resonances, which are exchanged in the intermediate states in the s-, t-, and u-channel, respectively. Parameters of the Lagrangian, masses, coupling constants and form factors, have to be taken either from other processes or have to be fitted to experimental data in the assumed process taking into account general principles such as SU(2) and SU(3) (broken at the level of $\approx 20\%$) symmetries.

The electro-magnetic structure of hadrons is modelled by various electro-magnetic form factors [8, 9] but the non point structure of hadrons in the strong vertexes was included only recently, for example in the Kaon-MAID [9], Janssen [11] and H2 [15] models. The hadron form factors (h.f.f.) are important for the proper description of the process at photon lab energies larger than 1.5 GeV since they suppress the cross section as a function of energy. In the models without h.f.f. which still provide reasonable results, e.g. Saclay-Lyon [8], the suppression is realized by inclusion of some hyperon resonances and nucleon resonances with higher spin ($3/2$ and $5/2$). The Williams-Ji-Cotanch (WJC) [10] model, in which h.f.f. are not assumed and which includes only one hyperon resonance, overpredicts the photo-production cross sections for photon energies larger than 2 GeV. Now, there are two main groups of these “isobaric” models which differ in the assumption of the hadronic form factors. Due to the dynamical content of the isobaric models (tree-level, masses of involved resonances are smaller than 2 GeV) their validity is limited to photon lab energy from the threshold up to 2.2 - 2.5 GeV.

In more elaborate approaches in which the unitarity is treated in a proper way all channels coupled to the process are assumed and described simultaneously [12]. These models are not, however, suited for practical purposes such as calculations of the production cross sections for hypernuclei. The model based on the Regge trajectory formalism [14], being derived for the photo-production process for energies larger than 5 GeV, was found to provide also reasonable results for the electro-production process for large enough photon mass ($Q^2 > 0.5 \text{ (GeV/c)}^2$). For the photo-production ($Q^2 = 0$) the Regge model systematically overpredicts the cross section for photon energies below 3 GeV. The very recent model based on the hybrid Regge-plus-resonance approach (RPR) [13] seems to be very promising for description of the forward angle data on the cross section and polarization. In the model the background contribution is fixed by the high-energy photo-production data, assuming the Regge description, and a resonant structure, revealed by the low-energy data, is modelled by several s-channel resonances as in the isobaric model.

Description of the elementary process is, however, very bad in the kinematical region relevant for the hypernuclear calculations for photon energies larger than 1.5 GeV and very small photon mass ($Q^2 \approx 0.06 \text{ (GeV/c)}^2$ - almost a real photon), which covers very forward kaon angles (small momentum transfer). Calculations of the cross section for production of hypernuclei in excited states, e.g. to analyze data from the hypernuclear experiments carried out in Jefferson Lab-

oratory, depend on two main ingredients, the elementary-production operator and the nuclear and hypernuclear structure information. To learn more on the hypernuclear structure, which is closely connected with the hyperon-nucleon interaction, one has to get uncertainty regarding the elementary process well under control, at least in the relevant kinematical region. Now, however, predictions for the hypernuclear production cross sections using various isobaric models for the elementary operator differ by more than 100% for kaon laboratory angles less than 10 degrees and photon energies larger than 1.5 GeV. The best result for production of ${}_{\Lambda}^{12}\text{B}$ hypernucleus was achieved with the SLA model, see section 2 for more details.

In the region of very forward angles the isobaric models provide two groups of substantially different results for the photo-production cross section, see Fig. 6 where predictions of the models discussed above are compared with new experimental data from CLAS [16], SAPHIR [18], and LEPS [17] Collaborations. An updated version of the hybrid RPR-2 model [13] (Regge-isobar approach) is shown in which P11(1900) resonance is replaced by D13(1900) one to better describe the latest data. The models with h.f.f., Kaon-MAID, Janssen C, and H2 [15], reveal very sharp damping of the cross section at kaon c.m. angles smaller than 30 degrees whereas the models without h.f.f., Saclay-Lyon and Williams-Ji-Cotanch (WJC) [10], continue in rising (Fig. 6). The CLAS and SAPHIR data suggest a plateau at these forward angles.

The phenomenon of damping the cross section can be understood based on analysis of the Saclay-Lyon A (SLA) and H2 [15] models at very forward angles and photon lab energy of 2 GeV. The cross section calculated with these models is dominated by the Born terms, particularly by the electric part of the proton exchange, at kaon c.m. angles smaller than 30 deg. This contribution provides a plateau in the cross section as the angle goes to zero for the SLA results. This feature would be very similar in both models since the main two coupling constants are almost equal. The situation is, however, different in H2 model due to very strong suppression of the proton term by h.f.f., which is of the order of 0.002 in the cross section for this energy region. In this region, the resonances contribute only in interference with the Born terms so that they cannot fill in the dip. The very strong suppression of the Born terms leads, therefore, to a pronounced dip in the differential cross section at very small angles (see Fig. 6 for the results of the H2 model). The Kaon MAID model gives a very similar result.

It seems that the strong suppression of the cross section at very forward angles and energies above 1.7 GeV is a common feature of the isobaric models with h.f.f. This dynamical aspect of the isobaric models desires therefore a more detailed investigation. However, the large bulk of new good quality experimental data cannot discriminate the models due to lack of data points at very forward angles. These latest data were measured only for c.m. kaon angles as small as 18 and 26 degrees for the LEPS or SAPHIR and CLAS sets, respectively, see Fig. 6 for illustration. Moreover the CLAS and SAPHIR data are not fully consistent at the forward angles, see Fig. 6

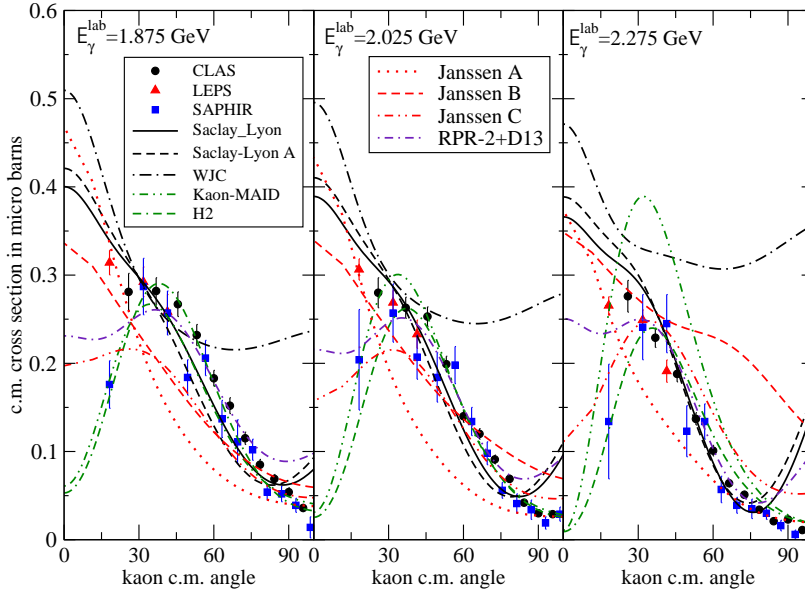


Figure 6: Predictions of some isobaric models are compared with experimental data.

and Ref.[16]. Since these data cannot discriminate the models, new high precision data on the photo-production are vital to solve the problem.

Moreover, the recent analysis of CLAS data on the cross section in a wide energy interval [16] shows beside the forward peaking also a progressive flattening of the slope as the kaon angle goes to zero. The CLAS data span, however, only to 26 degrees of kaon c.m. angle. The question whether the data continue in rising, form a plateau or drop down, as is the case for the high-energy (over 5 GeV) data [14] and as some of the models predict, is therefore another challenging question.

On the top of that there is urgent need for a very good description of the elementary operator at very forward angles which serves as input information in the hypernuclear calculations. The scarceness of data at forward angles can result only in a poor improvement in the description of the process and therefore in insufficient reduction of the uncertainty in the hypernuclear calculations. Call for another high quality data at very small kaon angles, which would help to elaborate the models, is therefore evident.

The Hall A apparatus is very suitable for performing such an experiment. Assuming kinematics similar to that of our previous measurement: beam momentum of 3.66 GeV/c, final electron momentum of 1.44 GeV/c, electron angle of 6 degrees, kaon momentum of 1.96 GeV/c, and kaon angle versus beam fixed at 6. (*already measured*), 8.5, and 11. degrees, suggests that

kaon laboratory angle versus the photon can be as small as 2.1, 4.6, and 7.1 degrees which in the c.m. frame is 5.4, 11.9, and 18.4 degrees, respectively. This measurement at photon energy of 2.2 GeV and for almost the real photon ($Q^2 = 0.06 \text{ (GeV/c)}^2$) can contribute significantly to the discussion on validity of predictions of various models for the elementary process in the kinematical region of interest and can, therefore, strengthen the predictive power of hypernuclear calculations.

The proposed kinematical region of measurements is indicated by the dotted vertical lines in Figure 7. The expected statistical uncertainties of 3% are indicated by the error bar at the “hypothetical” data points. The systematical uncertainty estimated on the basis of our previous experiment (E94-107) is below 10%.

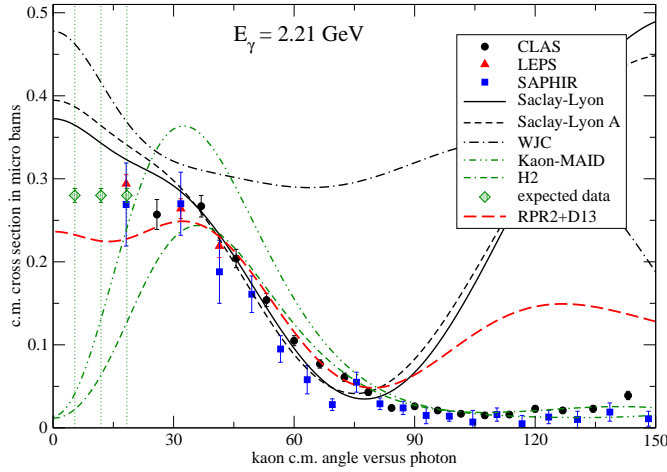


Figure 7: Predictions of some isobaric and the hybrid RPR-2 models are compared with experimental data. Positions of the proposed measurements are indicated by vertical dotted lines.

This experiment will contribute to a solution of the following questions:

- Does the cross section the photo-production continue to rise as the kaon angle goes to zero or is there a plateau (or a dip) ?
- Is the concept of the hadronic form factors as it is used in the isobaric models still correct for photon energies above 1.7 GeV?
- Which of the models describes better the reality at forward angles and can be therefore used in analysis of hypernuclear data without introducing an additional uncertainty?

Answers to these questions are very important for our understanding of the dynamics of the

process and the third one is even vital for the hypernuclear calculations since the elementary amplitude scales their predictions.

However, trying to solve these questions one has to keep in mind that in the Hall A experimental setup one will not measure the photoproduction cross section but the *electroproduction* one

$$\frac{d^3\sigma}{dE'_e d\Omega'_e d\Omega_K} = \Gamma \frac{d\sigma}{d\Omega_K}, \quad (2.1.1)$$

where Γ is the virtual photon flux and

$$\begin{aligned} \frac{d\sigma}{d\Omega_K} = & \frac{d\sigma_T}{d\Omega_K} + \epsilon_L \frac{d\sigma_L}{d\Omega_K} + \epsilon \frac{d\sigma_{TT}}{d\Omega_K} \cos 2\Phi_K + \sqrt{2\epsilon_L(1+\epsilon)} \frac{d\sigma_{TL}}{d\Omega_K} \cos \Phi_K \\ & - h \sqrt{2\epsilon_L(1-\epsilon)} \frac{d\sigma_{TL'}}{d\Omega_K} \sin \Phi_K, \end{aligned} \quad (2.1.2)$$

is the photoproduction cross section by virtual photons, ϵ/ϵ_L being transverse/longitudinal polarization of virtual photon.

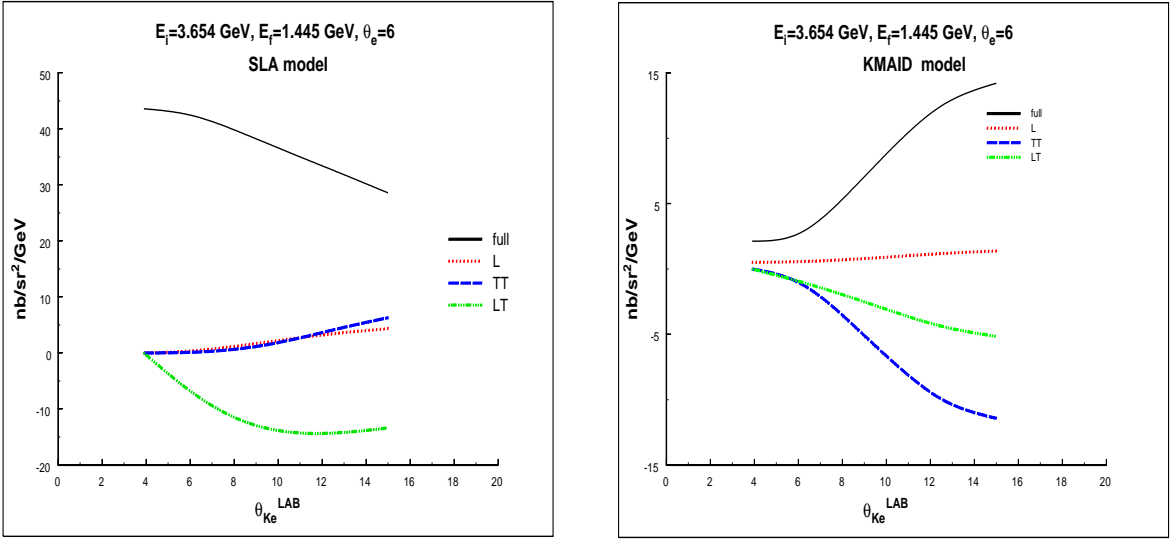


Figure 8: Triple differential cross section at $\theta_e = 6^\circ$, $E_i = 3.66$ GeV $E_f = 1.44$ GeV as a function of kaon laboratory scattering angle $\theta_{K_e}^{LAB}$ with respect to electron beam. At starting point $\theta_{K_e}^{LAB} = 3.9^\circ$ kaons are moving along the virtual photon momentum $\theta_{K_\gamma}^{LAB} = 0$. The left and right panels are for SLA and Kaon-MAID models, respectively.

The different pieces of the virtual photon cross section (2.1.2) can be interpreted as unpolarized transverse cross section (σ_T), cross section by longitudinally polarized photons (σ_L), transversely polarized photons (σ_{TT}), transverse-longitudinal interference term (σ_{TL}) and elec-

tron helicity contribution ($\sigma_{TL'}$). These contributions can be expressed in terms of standard CGLN-like amplitudes generated by the above mentioned models [8, 7].

At standard kinematical conditions (beam, final electron energy, and electron scattering angle) used in Hall A E94-107 hypernuclear experiment

$$E_i = 3.564 \text{ GeV}, \quad E_f = 1.454 \text{ GeV}, \quad \theta_{Ke} = 6^\circ, \quad (2.1.3)$$

the virtual photon 4-momentum squared $-p_\gamma^2 = Q^2 = 0.058 \text{ (GeV/c)}^2$, virtual photon flux $\Gamma = 0.0172$, polarizations $\epsilon = 0.681, \epsilon_L = 0.008$ and virtual photon angle (with respect to the electron beam) $\theta_{\gamma e} = 3.9^\circ$. This means that virtual photons are “almost real” (Q^2 being much smaller than involved masses of hadrons and energies) and contribution of longitudinal photons should be small (small ϵ_L). The interference terms σ_{TT} and σ_{TL} predicted by various models are exactly zero at $\theta_{K\gamma} = 0$ ($\theta_{Ke} = 3.9^\circ$) but they can be significantly large at $\theta_{Ke} \approx 10^\circ$ and strongly model dependent, see Fig. 8. However, we believe that utilizing the data distribution in the azimuthal angle Φ_K in (2.1.2) within the detector acceptance it will be possible to estimate the contribution of the interference terms. Anyway, the triple differential cross section Eq. (2.1.1) will be dominated by the contribution σ_T by transverse photons which in $Q^2 \rightarrow 0$ limit is the photoproduction cross section.

For in-plane kinematics ($\Phi_K = 180^\circ$) the situation is illustrated in Fig. 8. The used models are typical representatives of both groups (without and with hadron form factors) - SLA and Kaon-MAID. In addition to the full $d^3\sigma$ electroproduction cross section also the longitudinal and both interference terms are shown.

One can see that the longitudinal (L) contribution is really rather small in the whole angular range but at higher kaon scattering angles LT and TT interference terms can contribute significantly to the cross section as predicted by SLA/Kaon-Maid models. However, as mentioned above, they can be estimated by the out-of-plane angular dependence within the acceptance. This has to be carefully taken into account in the process of data analysis.

Finally, in Fig. 9 we show the electroproduction cross sections predicted by SLA, WJC, Kaon-Maid and H2 models. One can see that the characteristic small-angle behavior of the photoproduction cross section predicted by the same models is clearly seen also in the electroproduction process. The triple differential cross section predicted by the models without h.f.f. (SLA and WJC) is 20-40 nb/sr²/GeV which could be easily measured in Hall A. Our preliminary result from the E94-107 experiment is 23 nb/sr²/GeV.

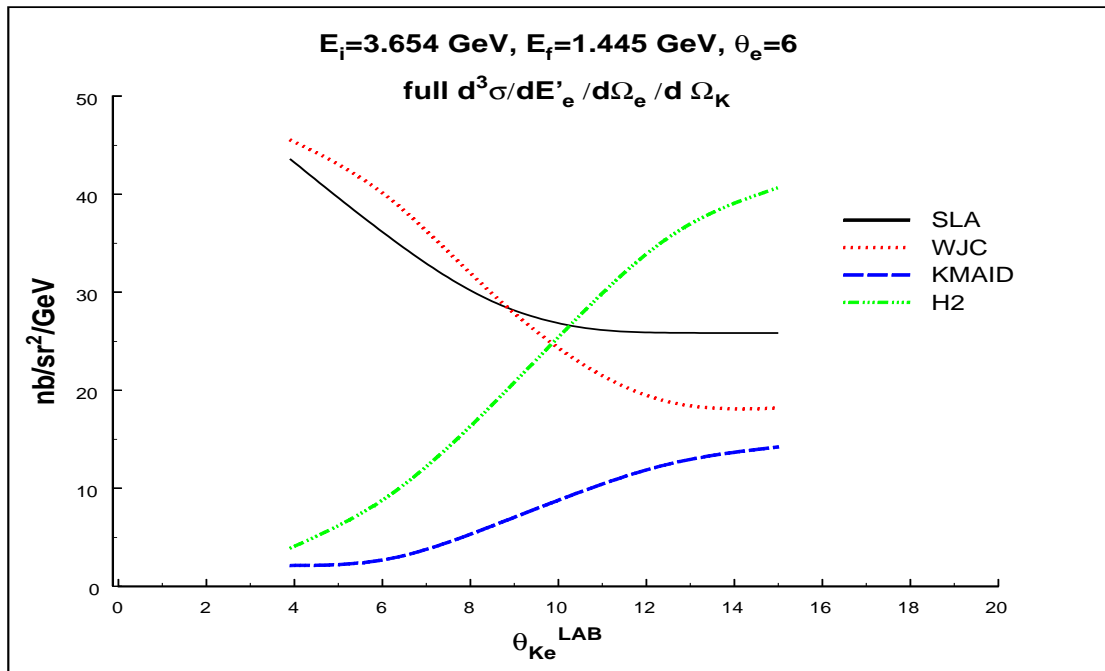


Figure 9: Triple differential cross section predicted by SLA, WJC, Kaon-Maid and H2 models.

3.2 Measurement of the Angular Dependence of the Cross Section for the Kaon Electroproduction on Oxygen

As we already mentioned the waterfall target gives a unique opportunity to simultaneously measure elementary and hypernuclear production cross sections and to obtain almost model independent information on the process. The angular dependence of the hypernuclear cross section is influenced mainly by the rapidly increasing momentum transfer to the nucleus with increasing kaon scattering angle. However, the deep dip predicted by some models with hadronic form factors can change the situation. In Figs. 10 and 11 we show angular dependencies of the hypernuclear production on the ^{16}O target predicted by SLA and Kaon-MAID models for four strongly populated peaks in the $^{16}_{\Lambda}\text{N}$ spectrum. What can one learn from these figures?

- The cross sections predicted by Kaon-MAID (and similar) models are approximately one order of magnitude smaller than those predicted by the SLA model;
- The Kaon-MAID model predicts again a dip at forward scattering angle in contrast to the SLA model which shows a monotonic decrease of the cross section due to the increasing momentum transfer;
- The slope of the angular shape depends rather strongly on the spin of the produced hypernuclear state. This effect is especially pronounced for $J = 1^-, 2^-$ members of first

excited doublet at excitation energy $E_x \simeq 7$ MeV and for $J = 1^+, 2^+$ members of the multiplet at $E_x \simeq 11$ MeV. Moreover, the cross section on ^{16}O reflects the strength of the elementary amplitude at small angles. Excitation of hypernuclear states brings in a different combinations of the elementary amplitudes for different final states. For example the nuclear structure for a specific final state can emphasize either spin-flip or non-flip amplitudes, as well as combinations of them with different phases. Deviations from an exponential decreases of cross sections with q could be caused by interference between the different amplitudes.

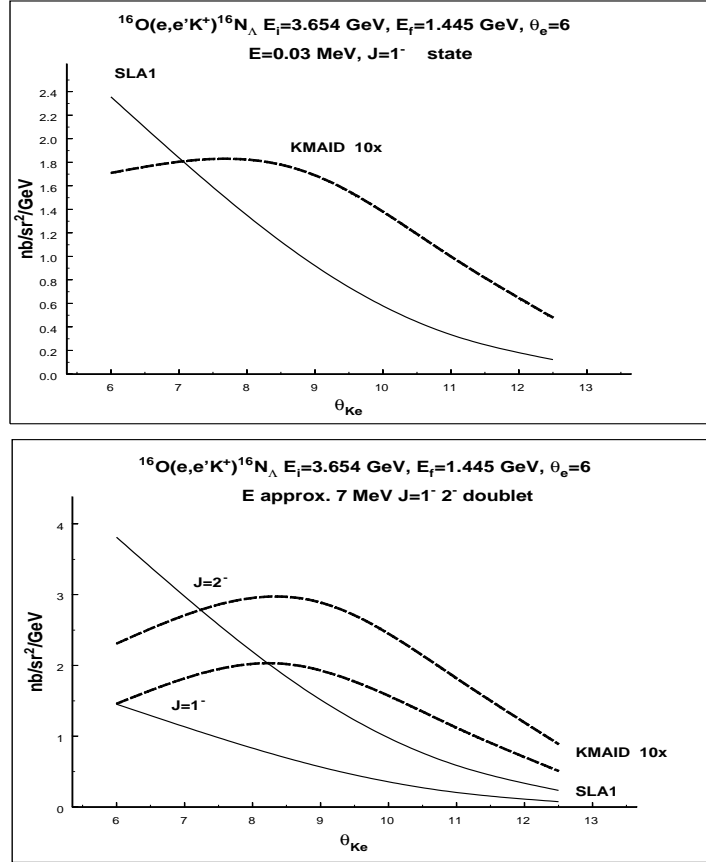


Figure 10: $^{16}\text{O}(e, e'K^+)^{16}\text{N}_\Lambda$ cross section for HN states with Λ in $s_{1/2}$ state as a function of kaon laboratory scattering angle θ_{Ke} .

Simultaneously measuring the electroproduction cross section on hydrogen and oxygen targets at a few kaon scattering angles can therefore not only discriminate between two groups of elementary models but it can shed new light also on some problems of hypernuclear physics.

In Figs. 12,13 we compare the preliminary results for the excitation spectra of the $^{16}_\Lambda\text{N}$ hypernucleus obtained in the previous experiment E94-107 (Fig. 12) with the projected measurements at different angles as they are predicted by the SLA ((Fig. 13 Left panel) and Kaon-MAID

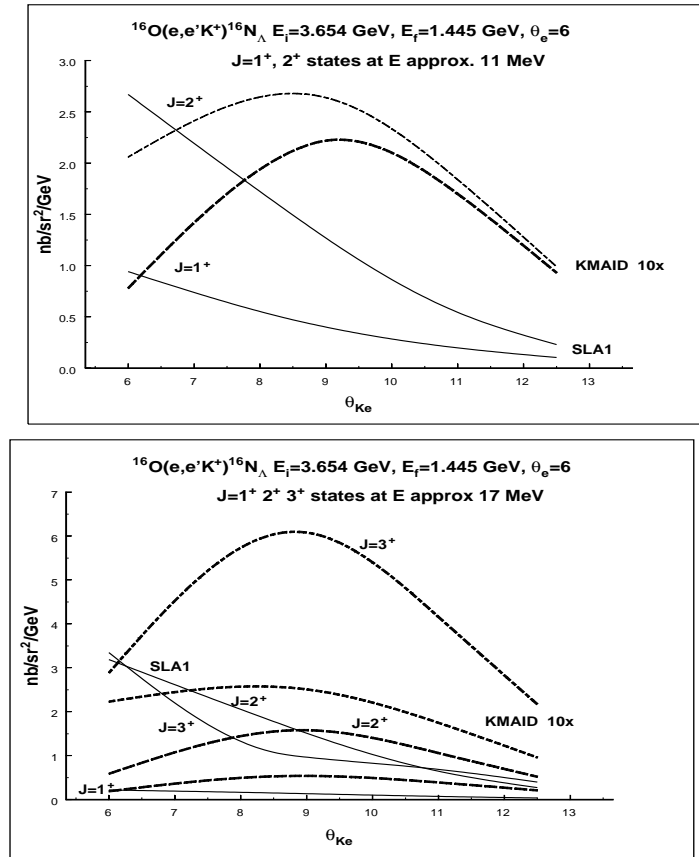


Figure 11: The same as Fig. 6 for HN states with Λ in $p_{3/2}, p_{1/2}$ states

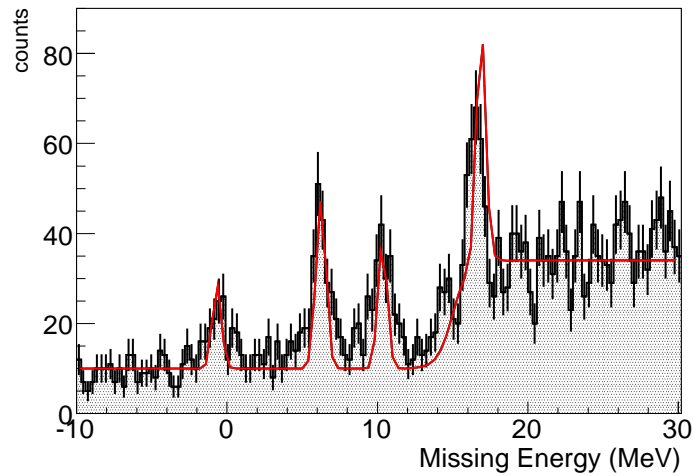


Figure 12: preliminary results for the excitation spectra of the $^{16}\text{N}_\Lambda$ hypernucleus obtained in the previous experiment E94-107

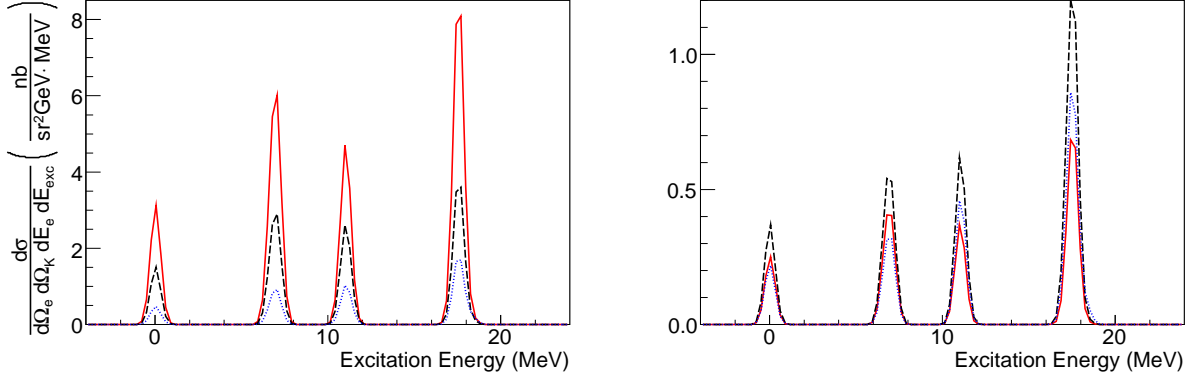


Figure 13: This proposal’s projected data according to two different models adopted for elementary $K^+ - \Lambda$ production on proton: SLA for the left panel; KMAID for the right panel. Solid lines are for $\theta_{K_e}^{LAB} = 6^\circ$, dashed lines for $\theta_{K_e}^{LAB} = 8.5^\circ$ and dotted line is for $\theta_{K_e}^{LAB} = 11^\circ$

(Fig. 13 Right panel) models. In this figure the solid line shows the calculation at 6° , the dashed line is for 8.5° and the dotted line is for 11° . It should be noted that while in the case of the SLA model the cross sections always decrease for larger angles, in the case of the KMAID model going from 6° to 8.5° they increase, then they decrease for 11° . The different dependence of the magnitudes of the peaks on the kaon angle is also apparent for the two models.

4 Experimental Apparatus, Kinematical Condition and Counting rates

As shown in experiment E94-107, Hall A at Jefferson Lab is well suited to perform (e,eK^+) experiments (see Fig.2). In that experiment scattered electrons at 6° were detected in the HRS right arm and coincident kaons were detected in the HRS left arm at 6° as well[2] . In the proposed experiment we will to match as well as possible the kinematical conditions of E94-107. This kinematics was used for E94-107 and the extension of this measurement at different Kaon scattering angles will produce precise measurement of angular dependences.

The only significant difference between that setup and the one proposed here is the movement of the kaon (left) arm to 8.5° and 11° . The septum magnets were specifically designed to allow detection out to 12.5° , accomplished by a small displacement and rotation of the septum magnet with no movement of the target location. Indeed, experiment E97-110, measuring the GDH sum rule, used the right septum at 9° . The left septum has already been trained up to 375 Amps, 34 Amps more than the anticipated 341 Amps needed to get 2.0 GeV/c at 12.5° . In the previous experiment, E94-107, $\sim 100 \text{ mg/cm}^2$ ^{12}C and ^9Be targets were used with an electron beam current of $\sim 100 \mu\text{A}$. For the waterfall target we used a thickness of $\sim 130 \text{ mg/cm}^2$ with a $50 \mu\text{A}$

beam current.

In the proposed experiment the choice of the same conditions for the energy and quality of the incident beam are requested. A beam current of $100 \mu A$, higher with respect to exp. E94-107 can be used since single rates are lower and this minimizes the running time by keeping the RICH detector and VDC efficiencies high.

The detector packages for the electron and hadron spectrometers are almost identical (described in [19]), except for the particle identification (PID) systems discussed later.

Incident Electron Energy	3.65 GeV
Virtual photon energy	2.2 GeV
Q^2	$0.0789 \text{ GeV}^2/c^2$
Electron scattering angle θ_e	6°
Kaon scattering angle θ_K	$8.5^\circ, 11.0^\circ$
Kaon momentum $ \vec{p}_K $	1.96 GeV/c
Electron momentum	1.45 GeV/c

Table 4: The kinematics of the proposed experiment.

Single rates, primarily from the (e, e') , (e, p) and (e, π^+) reactions, cause accidental coincidences which are the source of background for the experiment. This background of pions and protons, however, is completely suppressed using the Particle Identification apparatus, therefore the only remaining source of accidental background is the $(e, e')(e, K^+)$ reaction. Estimated rates are summarized in Table 5.

Angle	Singles					Accid.	Coinc.	Coinc
	(e, e')	(e, p)	(e, π^+)	(e, K^+)	(e, π^-)	$(e, e')(e, K^+)$	$p(e, e' K^+) \Lambda$	$^{16}\text{O}(e, e' K^+)_{\Lambda}^{16}\text{N}$
(deg)	(kHz)					$(h \times \text{MeV})^{-1}$	$(h)^{-1}$	$(h \times \text{MeV})^{-1}$
8.5	112	6.6	29	0.7	39	3.1	48	$\sim 0.8 - 2.0$
11	112	5.2	15.2	0.4	39	1.7	43	$\sim 0.4 - 1.0$

Table 5: Expected single, accidental, and real coincidence rates of the proposed experiment. Accidentals are for 3-ns gate in a 1 MeV energy bite.

4.1 Particle Identification

The identification of kaons detected in the hadron arm together with a huge background of protons and pions is one of the major challenge of the experiment. To reduce the background level in produced spectra, a very efficient PID system is necessary for unambiguous kaon identification.

In the electron arm, the Gas Cherenkov counters give pion rejection ratios up to 10^3 . The

dominant background (knock-on electrons) is reduced by a further 2 orders of magnitude by the lead glass shower counters, giving a total pion rejection ratio of 10^5 . The lead-glass shower counters and the gas Cherenkov are calibrated against each other.

The PID system in the hadron arm is composed of:

- two aerogel threshold Cherenkov counters A1 and A2 [21, 19] ($n_1 = 1.015$, $n_2 = 1.055$) (online and offline)
- the upgraded RICH detector (offline).

In the aerogel counters, charged pions (protons) with momenta around 2 GeV/c are above (below) the Cherenkov light emission threshold. Kaons emit Cherenkov light only in the aerogel with the higher index of refraction. Hence, the combination (coincidence, anticoincidence, absence) of the signals from the two counters distinguishes among the three species of hadrons. The A1 and A2 aerogel radiator were rebuilt (in summer 2005) and their performance is close to the design level with an online π :K (and p:K) rejection near 1:100.

The existing RICH detector will be also used to reach (offline) the required lower rejection of 1:1000 at least.

The RICH operated successfully during the E94-107 hypernuclear experiment providing a very satisfactory pion/kaon rejection at 2 GeV/c better than 1:1000 (corresponding to a pion/kaon angle separation larger than 5.0 sigma). The layout of the RICH is conceptually identical to the ALICE HMPID design [22]. It uses a proximity focusing geometry, a CsI photocathode, and a 15 mm thick liquid Freon radiator. A detailed description of the layout and the performance of the detector is given in [23, 24, 25].

The RICH detector is going to be upgraded to match the needs of the Transversity approved experiment (E06-011) to be able to identify kaons of 2.4 GeV/c, the photon detection plane will be doubled (3 more pad panels added) as shown in the MonteCarlo generated figure 14. This will allow the detectors to separate kaons, in our kinematical conditions (kaon momentum around 2 GeV/c) with a higher rejection ratio.

Therefore the proposed experiment will benefit both from rebuilt aerogel counters and above all from the upgraded RICH. According to the MonteCarlo simulation tuned on E94-107, the performance of the RICH alone will exceed the current Cherenkov angle separability by an additional ~ 1.5 sigma (see Fig. 15) corresponding to a pion:kaon rejection better than 1:10000 at 2.0 GeV/c, with improved efficiency.

Single rate events will be largely acceptable for the RICH detector; the acquisition rate of the RICH can sustain 800 Hz (far above the expected trigger rate after A1 and A2 anticoincidence selection) with a dead time smaller than 10 %.

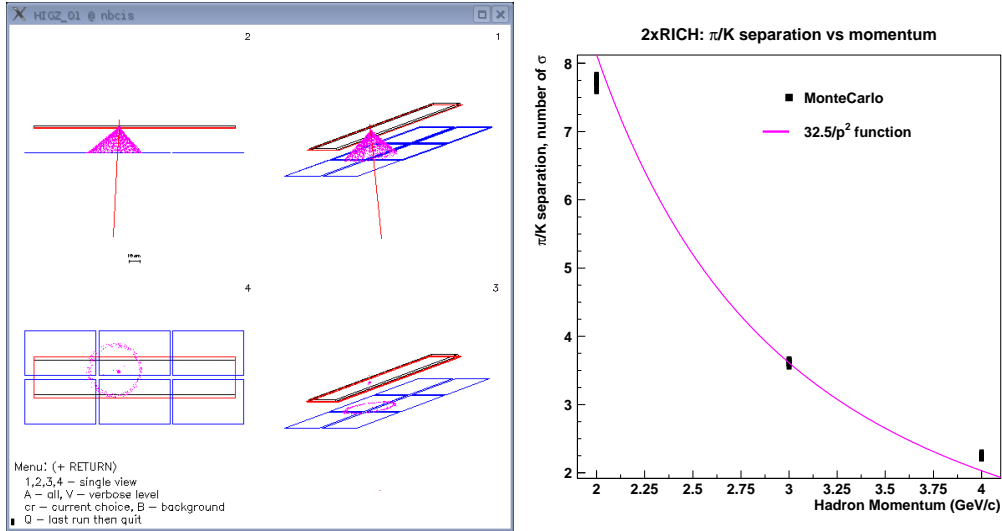


Figure 14: Upgraded RICH simulated event (Left panel) and expected performance (Right panel): Pion/Kaon angle separation (in terms of number of sigma) at different hadron momenta. Simulation is tuned to the existing Hypernuclear experiment data.

4.2 Calibrations and Detector Commissioning

We need to take data to optimize the optics reconstruction elements at each angle. The measurements proceed quickly, but require elastic scattering (i.e., an incident beam energy of ~ 1.6 GeV). The optics measurements will use ^{12}C , Ta, and H_2O targets. Sieve slit data will be taken to determine the angular matrix elements. A delta scan will determine the momentum dependence of the optics elements. Beam angle, bullseye, raster size, and incident energy shifts will also be measured. The data comes in quickly however and 16 hours total has been allocated for optics elements. This measurement uses electrons in both arms as well.

In addition to determining the optics, elastic scattering data from the H_2O target is also needed at different pump speeds to determine the absolute target thickness. This only needs to be done at one angle. Since the electron arm stays fixed throughout the experiment, it forms a luminosity monitor for the measurement. An additional 8 hours is needed the target thickness measurement. This measurement will be done with electrons in both arms, with the single arm cross sections forming two independent measurements of the target thickness.

Finally, detector checkout is needed with coincidence data to optimize scintillator offsets, check timing gates, adjust RICH HV, and measure PID efficiencies. An additional 24 hours is listed for coincidence checkout.

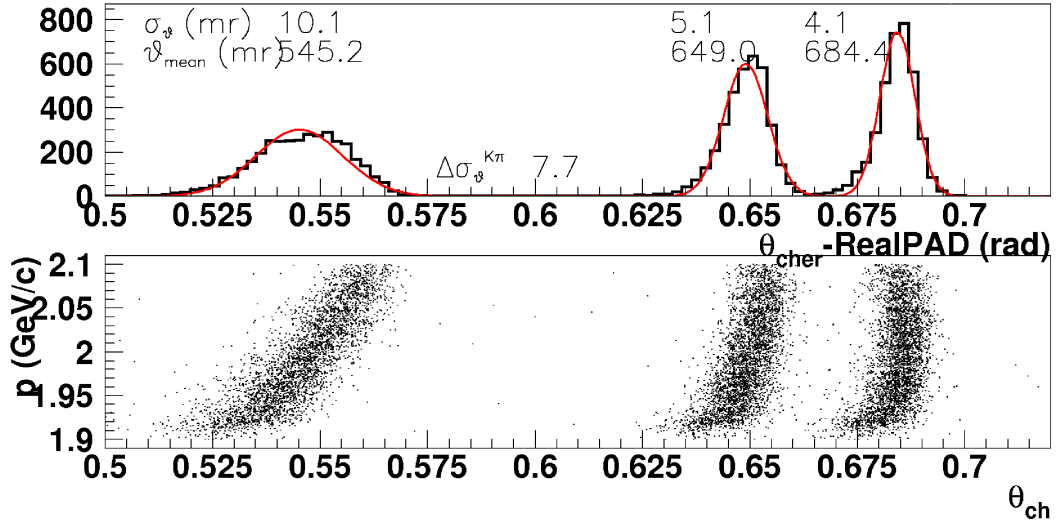


Figure 15: Upgraded RICH simulated performance: Pion/Kaon angle distribution (equal hadrons population) at 2.0 GeV/c momentum, in the HRS acceptance ($\pm 5\%$). The Monte-Carlo is tuned to the existing Hypernuclear experiment data.

5 Beam time request

Table 6 lists the beam time request. The right HRS+Septum stays at 6° but the left HRS+Septum changes from 8.5 to 11° . The waterfall thickness is 130 mg/cm^2 for both angles and the beam current is $100 \mu \text{ A}$

Purpose	Energy	Time
Calibrations	1.6 GeV	2 days
8.5°	3.66 GeV	7 days
11°	3.66 GeV	15 days
Total		24

Table 6: Beam Time Request.

6 Summary

The cross section on ^{16}O reflects the strength of the elementary amplitude at small angles. Excitation of hypernuclear states brings in a different combinations of the elementary amplitudes for different final states. For example the nuclear structure for a specific final state can emphasize either spin-flip or non-flip amplitudes, as well as combinations of them with different phases. Deviations from an exponential decrease of cross sections with q could be caused by interference between the different amplitudes. The experiment will answer the following questions:

- What is the angular dependence of the hypernuclear form factor, particularly at forward angles where the models sharply disagree?
- Is the hypernuclear angular dependence the same as the elementary angular dependence?

Measurement of the elementary cross section at forward angles are very difficult to reach in other laboratories, but are needed to solving the following questions:

- Does the cross section for photo-production continue to rise as the kaon angle goes to zero or is there a plateau (or even a dip)?
- Is the concept of hadronic form factors as it is used in the isobaric models correct? For photon energies above 1.7 GeV it has not been measured and at all energies, forward angle information is missing.
- Which of the models describes the reality at forward angles and therefore can be used in analysis of hypernuclear data without introducing an additional uncertainty?

Answers to these questions are very important for our understanding of dynamics of the process. The third one is also vital for hypernuclear calculations since the elementary amplitude scales these hypernuclear calculations predictions.

References

- [1] O. Hashimoto and H. Tamura, *Prog. Part. Nucl. Phys.* **57**, 405 (2006).
- [2] F. Garibaldi, S. Frullani, P. Markowitz, and J. LeRose, spokespersons, JLab Experiment E94-107, High Resolution 1p shell Hypernuclear Spectroscopy (1994).
- [3] C. Milner et al. *Phys. Rev. Lett.* **54** (1985) 1237.
- [4] H. Hotchi *et al.*, *Phys. Rev. C* **64**, 044302 (2001).
- [5] M. Agnello *et al.*, *Phys. Lett. B* **622**, 35 (2005).
- [6] T. Miyoshi *et al.*, *Phys. Rev. Lett.* **90**, 232502 (2003); L. Yuan *et al.*, *Phys. Rev. C* **73**, 044607 (2006).
- [7] M. Sotona and S. Frullani, *Prog. Theor. Phys. Suppl.* **117**, 151 (1994).
- [8] J.C. David, C. Fayard, G.-H. Lamot, B. Saghai, *Phys. Rev. C* **53**, 2613 (1996); T. Mizutani, C. Fayard, G.-H. Lamot, B. Saghai, *Phys. Rev. C* **58**, 75 (1998).

- [9] T. Mart and C. Bennhold, Phys. Rev. C **61**, 012201 (1999); C. Bennhold *et al.*, nucl-th/9901066.
- [10] R.A. Williams, Chueng-Ryong. Ji, and S.R. Cotanch, Phys. Rev. C **46**, 1617 (1992).
- [11] S. Janssen, J. Ryckebusch, D. Debruyne, T. Van Cauteren, Phys. Rev. C **65**, 015201 (2001).
- [12] G. Penner and U. Mosel, Phys. Rev. C **66**, 055212 (2002).
- [13] T. Corthals, J. Ryckenbusch, T. Van Cauteren, Phys. Rev. C **73**, 045207 (2006); the calculations by private communication.
- [14] M. Guidal, J.-M. Laget, M. Vanderhaeghen, *Nucl. Phys.* **A627**, 645 (1997); *Phys. Rev.* **C61**, 025204 (2000).
- [15] P. Bydžovský and M. Sotona, Nucl. Phys. A **754**, 243c (2005); nucl-th/0408039.
- [16] R. Bradford et al (CLAS Collaboration), Phys. Rev. C **73**, 035202 (2006).
- [17] M. Sumihama et al (LEPS Collaboration), Nucl. Phys. A **754**, 303 (2005).
- [18] K.-H. Glander *et al.*, Eur. Phys. J. A **19**, 251 (2004); nucl-ex/0308025.
- [19] J. Alcorn *et al.*, Nucl. Instrum. Methods A **522**, 294 (2004).
- [20] G.M. Urciuoli, *et al.*, Nucl. Phys. **A691**, 43 (2001).
- [21] L. Lagamba *et al.*, Nucl. Instrum. Methods A **471**, 325 (2001).
- [22] CERN/LHCC 98-19, ALICE TDR 1, 14 August 1998
- [23] M. Iodice *et al.*, Nucl. Instrum. Methods A **553**, 231 (2005).
- [24] F. Garibaldi *et al.*, Nucl. Instrum. Methods A **502**, 117 (2003).
- [25] F. Cusanno *et al.*, Nucl. Instrum. Methods A **502**, 251 (2003).
- [26] M. Ukai *et al.*, Phys. Rev. C **73**, 012501 (2006).
- [27] D.J. Millener, Nucl. Phys. **A691**, 93 (2001).
- [28] F. Ajzenberg-Selove, Nucl. Phys. **A506**, 1 (1990).